The Electrochemical Society
Advancing solid state & electrochemical science & technology

Modelling of the Elementary Steps Involved in the Aluminum Electrochemical Deposition from Ionic Liquid Based Solution: The *BMImCl/AlCl₃* System

View the article online for updates and enhancements.

Modelling of the Elementary Steps Involved in the Aluminum Electrochemical Deposition from Ionic Liquid Based Solution: The *BMImCl*/*AlCl₃* System

Massimo Innocenti, [1,*] Andrea Giaccherini,[1] Riccardo Chelli,[1,2] Stefano Martinuzzi,[1] Walter Giurlani,[1] Maurizio Passaponti,[1] Alessandro Lavacchi,[3,*] and Claudio Fontanesi [4,z]

[1]*Department of Chemistry, University of Firenze, 50019 Sesto Fiorentino, Firenze, Italy*
[2]*European Laboratory for Non-Linear Spectroscopy (LENS), 50019 Sesto Fiorentino, Firenze, Italy*
[3]*CNR, ICCOM, 50019 Sesto Fiorentino (FI)*
[4]*Department of Engineering, DIEF, University of Modena and Reggio Emilia, 41125 Modena, Italy*

The energy hierarchy, of the main chemical species involved in the reaction mechanism relevant to the electrodeposition of aluminum in 1-Butyl-3-methylimidazolium chloride/aluminum trichloride solution (*BMImCl*/*AlCl₃*), is studied by using ab-initio based theoretical calculations. Eventually, a reasonable theoretical estimate of energies, involved in the principal reactions ruling the aluminum electrodeposition from *BMImCl* ionic liquid solutions, is obtained. For screening purposes (geometry optimization and Hessian calculations) the CAMB3LYP density functional, DFT, has been used. Then single point (exploiting CAMB3LYP optimized geometries) energy data are obtained at the Møller-Plesset (MP2) level of the theory. They are used to cross-check DFT results. A reaction mechanism emerges in which, although the species $AlCl_4^-$ is formed with very high efficiency from the neutral species $AlCl_3$, the competing reaction $AlCl_4^- + AlCl_3 \rightleftharpoons Al_2Cl_7^-$ points to an almost complete conversion of aluminum to the dimeric form into bulk solution. This is observed in the absence and, most importantly, in the presence of a coordinating BMIm⁺ cation. In this respect, the presence of BMIm⁺ does not seem to affect significantly the equilibrium between the monomeric and dimeric forms of aluminum. This outcome is very interesting because the dimeric species is directly reduced to yield the metal aluminum. Indeed, a larger concentration of $Al_2Cl_7^-$ gives due reason for a more effective electrodeposition process, as it is experimentally observed in the ionic liquid medium.

Since its invention, the Heroult-Hall process[1] has been the conventional process for the production of metallic aluminum. It is based upon the electroreduction of alumina on a cryolite melt by using graphite electrodes. The high temperature required (in the order of 900°C) and the emission of toxic gaseous by-products, such as fluorine and carbon monoxide, rendered the research for greener and safer alternative techniques highly attractive. The introduction of Ionic Liquids (ILs) (namely room temperature molten salts) as electrochemical media for the aluminum electrodeposition offered a very promising route to succeed in this goal. Since the first pioneeristic studies in the 1999,[2] a large number of investigations successfully reported the electrodeposition of aluminum, at lab scale, at room or nearly room temperature. Different type of ionic liquids,[3–7] ionic liquid mixtures and additives[8,9] were proposed to achieve the electrodeposition of Al-coatings. However, with the aim of the industrialization of the Al-plating process, chloroaluminate ionic liquids, without additives, seems to constitute the better compromise between the quality of the deposit and the stability and durability of the electroplating bath. Beside the handling difficulties, mainly due to the vigorous reaction with atmospheric moisture, their high aluminum content, reduced viscosity and remarkable electrochemical stability, allow to achieve high deposition rate; in the order of 10–20 μm h⁻¹ for these media, and long working time without maintenance or chemicals replenish.[8,10–12]

The Al-coatings obtained at lab scale by means of this technology have been successfully used as protective layers for structural materials such as carbon steel, magnesium alloys,[13] light weight alloys,[14] just to name a few. In recent years, several studies have been performed aiming at finding the optimal conditions for the electrodeposition of this protective coatings.[15,16]

The scale-up of the process have been attempted through different strategies, as reported by some us and elsewhere[17,18] an a priori assessment of the optimal conditions can be designed by means of finite element analysis (FEA). However, a general lack of structural and thermodynamic data about this IL limited the modelling of the electrodeposition to the sole transport processes impairing the simulation of the chemical process competing with the heterogenous reaction leading to the electrodeposition of Al from 1-Butyl-3-methylimidazolium chloride/aluminum trichloride solutions (BMImCl/AlCl₃). This study aims at clarifying some of the structural and thermodynamic aspects, at a molecular level, of the BMImCl/AlCl₃ system in DFT and MP2 post Hartree-Fock frameworks.

The Reaction Mechanism

Figure 1 shows the molecular structures of the ionic liquids studied in this paper.

Figure 2 sets out a pictorial representation of the main reactions involved in the *Al* electrochemical deposition process, when the latter is carried out in the *BMImCl*/*AlCl₃* Ionic Liquid medium. The main formation reactions of the monomer $AlCl_4^-$ and of the dimer $Al_2Cl_7^-$, from $AlCl_3$, are the following:

$$AlCl_3 + Cl^- \rightarrow AlCl_4^- \qquad [1]$$

$$AlCl_4^- + AlCl_3 \rightarrow Al_2Cl_7^- \qquad [2]$$
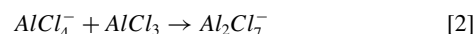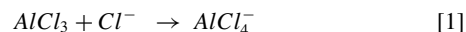
The electrodeposition of metallic *Al* on the cathode is completed by the charge transfer process:

$$4\,Al_2Cl_7^- + 3e^- \rightarrow 7\,AlCl_4^- + Al. \qquad [3]$$

In our study we mainly focused our attention on the thermodynamic equilibria 1 and 2, which occur within the massive IL bulk of the solution, and involving the species: Cl^-, $AlCl_3$, $AlCl_4^-$ and $Al_2Cl_7^-$. In particular, the effect of the presence of the cation $BMIm^+$ on the thermodynamic equilibrium is here studied. This aspect is tackled by comparing the value of the standard reaction free energies ΔG_f^0, relevant to Reactions 1 and 2. They can be inferred assuming as active species the anions Cl^-, $AlCl_4^-$, $Al_2Cl_7^-$ and the ionic couples $BMIm^+Cl^-$,

*Electrochemical Society Member.
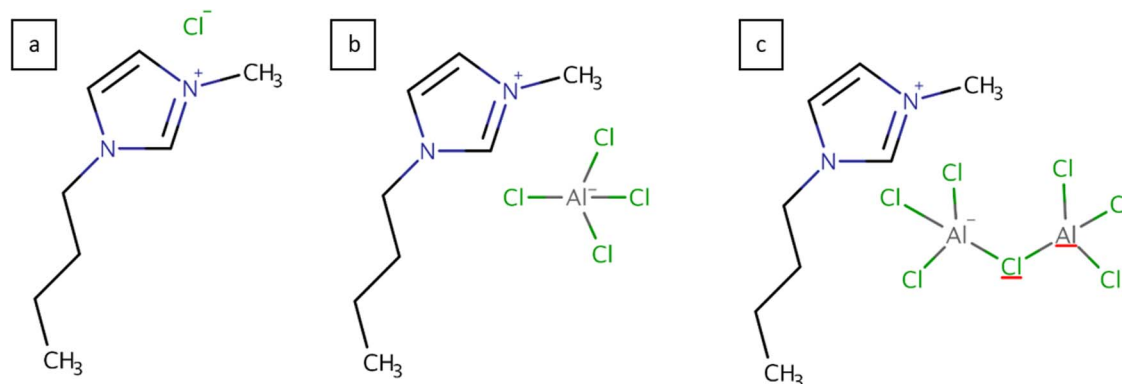ᶻE-mail: m.innocenti@unifi.it; claudio.fontanesi@unimore.it

Figure 1. Molecular structures of: (a) $BMIm^+Cl^-$ (b) $BMIm^+AlCl_4^-$ and (c) $BMIm^+Al_2Cl_7^-$.

$BMIm^+AlCl_4^-$, $BMIm^+Al_2Cl_7^-$. Please compare the reaction scheme reported in Figure 2. Thus, considering the relevant ionic couples, the 1 and 2 equilibrium reactions can be written as Reactions 1a and 2a:

$$AlCl_3 + BMIm^+Cl^- \rightarrow BMIm^+AlCl_4^- \qquad [1a]$$

$$BMIm^+AlCl_4^- + AlCl_3 \rightarrow BMIm^+Al_2Cl_7^- - \qquad [2a]$$
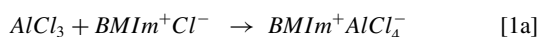
Computational Details

The standard formation Gibbs free energy, ΔG_f^0, of each reacting species has been estimated on the basis of DFT based theoretical calculations. For each reagent ΔG_f^0 is obtained as the weighted average between initial-not-equivalent optimized structures (here "initial-not-equivalent" means different initial geometrical molecular structures, "guess", for each single compound). The problem of the selection of a sufficient large number of initial-not-equivalent (randomly chosen) structures in yielding a significant representative number of sampled geometries, is particularly important for species presenting a flexible structure, like: $BMIm^+Cl^-$, $BMIm^+AlCl_4^-$, $BMIm^+Al_2Cl_7^-$. From a series of 20 randomized starting configurations, the number of initial-not-equivalent optimized structures is 4 for $BMIm^+Cl^-$, 14 for $BMIm^+AlCl_4^-$, and 16 for $BMIm^+Al_2Cl_7^-$. On the contrary, in case of not flexible species, Cl^-, $AlCl_4^-$, $Al_2Cl_7^-$, a single optimized structure was obtained. Quantum mechanical based calculations were carried out using the Gaussian 16 program.[19] Density functional theory (DFT) calculations were performed by using two different hybrid correlation-exchange functionals: CAM-B3LYP[20] and PBE0,[21] using the 6–31G(d) basis set. For the sake of a more complete comparison, single-point energy calculation at the MP2/TZVP level of the theory have been performed (single-point means selecting a fixed geometry structure which was obtained by full geometrical optimization, vide-supra, at the CAM-B3LYP/6-31G(d) and PBE0/6-31G(d) level of the theory). In our quantum mechanical based calculations the solvent effect is explicitly accounted for by using the Conductor-like Polarizable Continuum Model (CPCM) as implemented within the Gaussian 16 program.[19] Dielectric continuum theories are now widely used to describe solvation effects within quantum mechanical based calculations, this due to the relatively low cost of the calculation. For the ionic liquid the static and dynamic dielectric permittivity were selected as 11.5 and 2.05, respectively.

For each non-redundant optimized structure j of species i, the free energy G_{ij}^0 was calculated by the Gaussian16 program, including the translational, rotational, vibrational and electronic free energy contributions (following a vibrational, Hessian calculation, analysis). The electronic partition function was approximated accounting for only the ground state contribution. The total free energy of the species i was then given by the sum of the equilibrium weights $e^{-\beta G_{ij}^0}$ of each $j - th$ optimized conformer:[22]

$$G_i^0 = -\beta^{-1}\ln\left(\sum_j e^{-\beta G_{ij}^0}\right), \qquad [4]$$

where the sum runs over on the j non-redundant configurations. The calculation of the reaction free energy is given by the difference between the sum of the formation free energies of products and reagents:

$$\Delta G^0 = \sum_P n_P G_P^0 - \sum_R n_R G_R^0, \qquad [5]$$

where n_P and n_R are the stoichiometric coefficients of products and reagents, respectively.

Results and Discussion

Optimization and configuration analysis of $BMIm^+Cl^-$.—In the following we will refer to vectors defined as the difference between the position vector of two i and j atoms as $\|R_{i,j}\|$, where i and j are the sequential number of the atoms as depicted in Figure 3 for the $BMIm^+Cl^-$.

To specify the position of the Cl^- anion with respect to the $BMIm^+$ cation two angles, θ and ϕ, have been defined with respect to the aromatic ring plane (light blue plane shown in Figure 3b). The two angles are defined making reference to two suitably selected vectors, $R_{1,6}$ and $R_{14,6}$ (compare Figure 3), which take into account the distance of chlorine with respect to the imidazole ring. The deviation from coplanarity is accounted or the angle formed with the vector $R_{14,6}$ which is laying coplanar with the imidazole plane as depicted in Figure 3a:
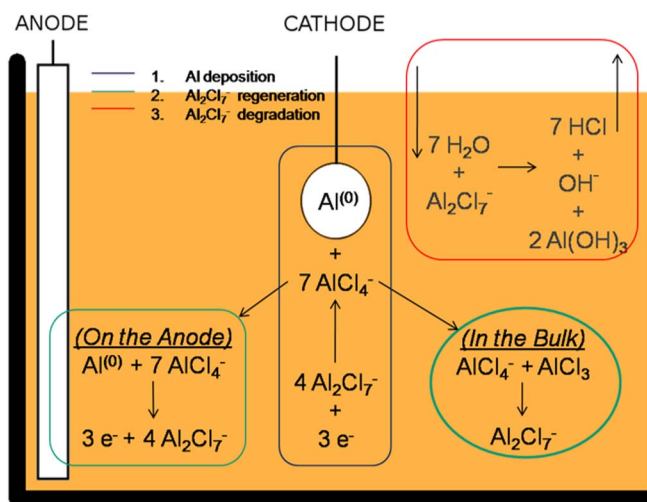

Figure 2. Schematic representation of the main chemical and electrochemical processes involved in the Al electrodeposition from *BMImCl* solution.
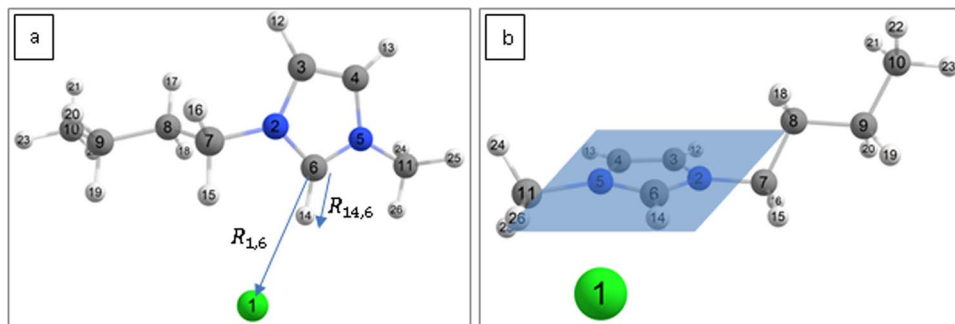
Figure 3. Schematic representation of the most frequent $BMIm^+Cl^-$ conformers (green center numbered 1 is the chloride anion). The most representative geometrical parameters are shown: (a) two relevant internal coordinates $\|R_{1,6}\|$ and $\|R_{14,6}\|$ and (b) the, imidazole moiety, aromatic plane.

(a) θ is the angle between the aromatic plane and the $R_{1,6}$ vector, the latter is defined with respect to carbon 6 of the imidazole ring and pointing toward the Cl^- anion.

(b) ϕ is the angle defined by the projection of the vector $R_{1,6}$ on the aromatic plane and the vector $R_{14,6}$.

Criteria underlying the choice of θ and ϕ: θ shows how much the Cl^- deviates in coplanarity with respect to the aromatic imidazole plane, ϕ takes into account the position of Cl^- with respect to the aromatic ring.

Figures 4a, 4b show the number of conformers as a function of the angles θ and ϕ. Figures 4c, 4d show the number of conformers as a function of the distance of the Cl^- anion from the atoms 6 and 4 ($\|R_{1,6}\|$ and $\|R_{1,4}\|$).

Optimization and configuration analysis of $BMIm^+AlCl_4^-$.— Note that concerning the optimization and configuration analysis of $BMIm^+AlCl_4^-$, angles θ and ϕ remain defined as in the previous paragraph: compare Figure 3. Then, the orientation of $AlCl_4^-$, with respect to the imidazole aromatic plane, is described by the dihedral angle depicted in Figure 5a. Figures 5a, 5b shows the two most frequent configurations of $BMIm^+AlCl_4^-$, where the $AlCl_4^-$ is located in two different positions on the aromatic plane. Figure 6 shows the distribu-

tion of the configurations for different angle and distances. Figure 6a confirms that the prominent most frequent disposition of the Al in $AlCl_4^-$ is on the aromatic plane. However, a wide distribution around this value is clearly present. Figure 6b shows the two main positions on the aromatic plane for the Al in $AlCl_4^-$ ($\phi = 0°$ and $\phi = 150°$). Figures 6c shows two main distance value distributions for $\|R_{1,10}\|$, corresponding to the two main configurations described by the distribution of the ϕ values. Figure 6d shows that there is no main value for the dihedral defined in Figure 5a.

Optimization and configuration analysis of $BMIm^+Al_2Cl_7^-$.— Angles θ, ϕ and the dihedral angle are defined similarly to the choice made in Optimization and configuration analysis of $BMIm^+Cl^-$ and Optimization and configuration analysis of $BMIm^+AlCl_4^-$ sections. The two most statistically dominant conformers are presented in Figure 7, where the $Al - Al$ distance, $\|R_{1,6}\|$, marks the different orientation of the $Al_2Cl_7^-$. Which can be parallel to the normal vector of the aromatic plane in the $BMIm^+$ cation or tilted by roughly 45°. This observation is quantitatively described by the conformer frequency distribution shown in Figure 8. Indeed, for $BMIm^+Al_2Cl_7^-$ is evident the presence of a bimodal distribution of conformers. This gives due reason to the ability of the geometrical parameters used in Figure 7 to discriminate between the main possible conformer structures. The
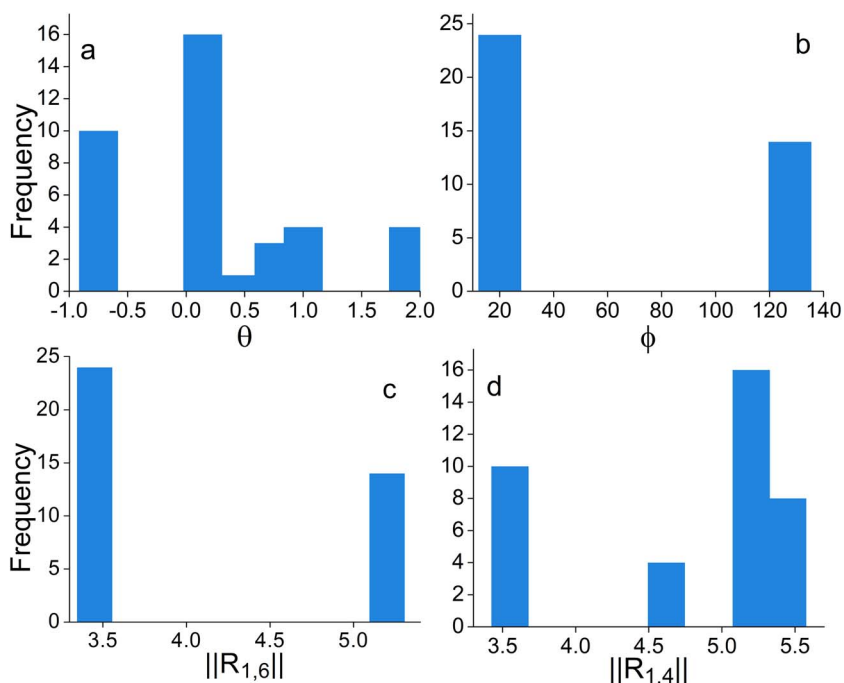

Figure 4. Histograms showing the number of conformers for the $BMIm^+Cl^-$ species as a function of (a) angle θ, (b) angle ϕ, (c) the distance between centers 1 and 6 (d) the distance between centers 1 and 4.

Figure 5. Schematic representation of the two most frequent $BMIm^+AlCl_4^-$ conformers (green centers are chloride anions) a) and b). The arrows in panel (a) show the dihedral angle between centers 1-4-10-9.

Figure 6. Histograms showing the frequency of (a) angle θ, (b) angle φ, (c) the distance between atom 1–10 and (d) the dihedral between the atoms 1-4-10-9 in $BMIm^+AlCl_4^-$.

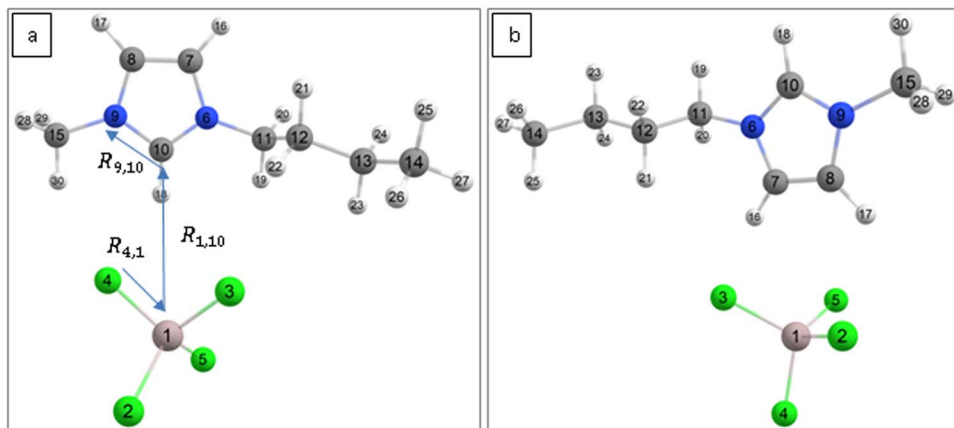**Figure 7.** Schematic representation of the two most frequent $BMIm^+Al_2Cl_7^-$ conformers (green centers are chloride anions)
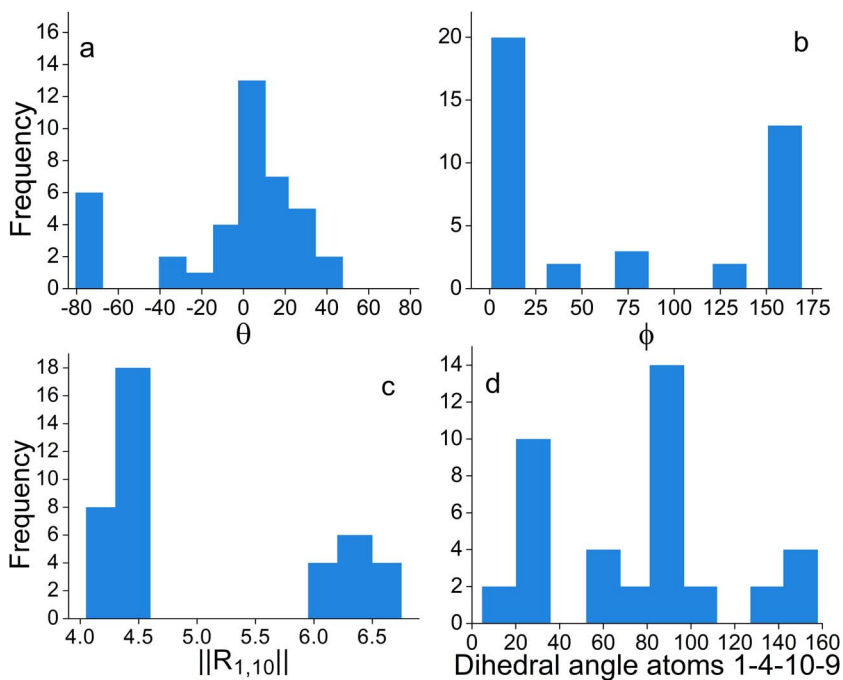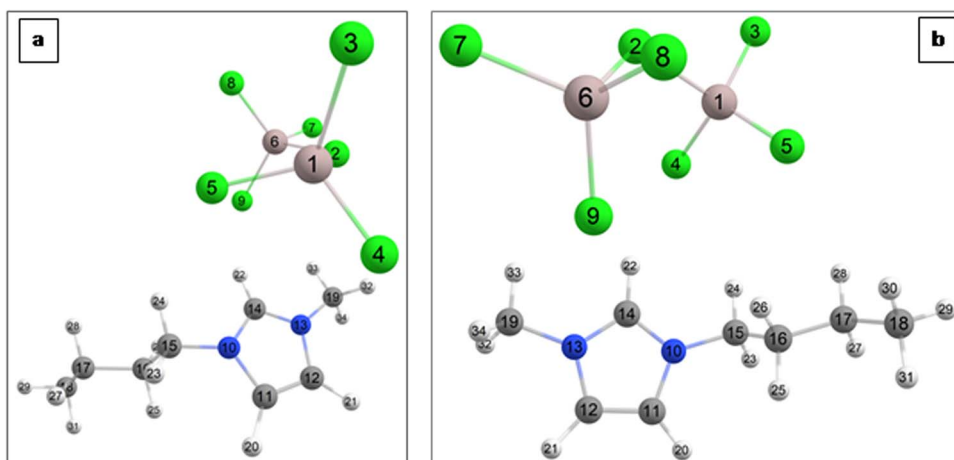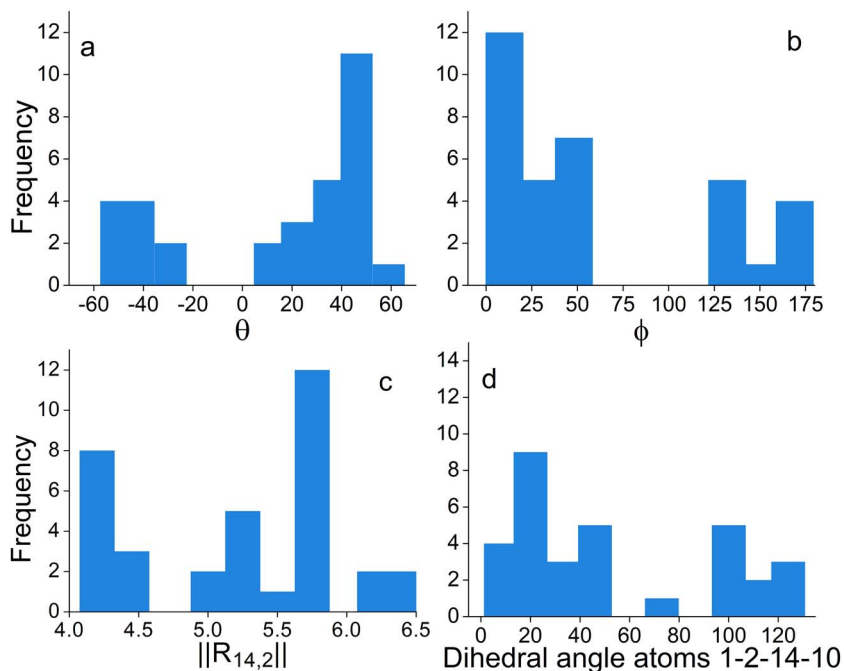
Figure 8. Histograms showing the frequency of (a) angle θ, (b) angle ϕ, (c) the distance between atom 2–14 and (d) the dihedral between the atoms 1-2-14-10 for the $BMIm^+Al_2Cl_7^-$.

Table I. Calculated Gibbs free energies (a.u.) of the different chemical species considered in the Al electrodeposition as a function of different DFT functionals, and with post-scf MP2 electron correlation correction.

Compound	CAMB3LYP/6-31G(d)	MP2/TZVP[1]	PBE0/6-31G(d)	MP2/TZVP[2]
Cl^-	−460.3740	−460.4087	−460.1831	−460.1941
$Al_2Cl_7^-$	−3706.9563	−3707.1830	−3705.357	−3705.4168
$AlCl_3$	−1623.2476	−1623.3475	−1622.5415	−1622.5698
$AlCl_4^-$	−2083.6967	−2083.8254	−2082.8019	−2082.8355
$BMImCl$	−883.1905	−883.3614	−882.6976	−882.62245
$BMImAl_2Cl_7$	−4129.7656	−4130.1285	−4127.8612	−4127.8333
$BMImAlCl_4$	−2506.5058	−2506.7709	−2505.3072	−2505.2544

[1]Single point calculation, geometry optimized at CAMB3LYP/6-31G(d) level of theory.
[2]Single point calculation, geometry optimized at PBE0/6-31G(d) level of theory.

same does not hold for the $Cl − C$ (2-14), $\|R_{1,14}\|$, distance parameter, compare Figure 8c.

Reaction Gibbs free energies.—In Table I are reported the free energies calculated for the different species present in the bulk ionic liquid solution. Results have been obtained through the procedure described in the Computational Details section, density functionals CAM-B3LYP and PBE0. For both the functionals, are reported data from optimization with the 6–31G(d) basis (a level of theory which already proved to yield reliable data when dealing with complex

charged systems[23,24]). Single-point (i.e. fixed geometries at the CAM-B3LYP/6-31G(d) and PBE0/6-31G(d) level of the theory). MP2/TZVP energies were also calculated for the sake of comparison.

Table II reports reaction free energies for the 1, 2, 1a and 2a reactions, allowing for a comparison of the free energy differences between products and reagents obtained by using different levels of theory.

As a general trend, the use of PBE0 functional stabilizes both monomer and dimer anions formation, toward CAM-B3LYP data (expected to be the better estimation of the intermolecular electrostatic interactions). Observing the reaction free energies of Reactions 1 and

Table II. Reaction free energies (kJ/mol).

Reaction	CAMB3LYP/6-31G(d)	MP2/TZVP[1]	PBE0/6-31G(d)	MP2/TZVP[2]
(1) $AlCl_3 + Cl^- \rightleftharpoons AlCl_4^-$	−197.3	−181.3	−202.3	−188.1
(1a) $AlCl_3 + Cl^- \rightleftharpoons BMImCl_4$	−177.8	−162.9	−178.9	−163.1
(2) $AlCl_3 + AlCl_4^- \rightleftharpoons Al_2Cl_7^-$	−31.5	−26.3	−37.3	−30.2
(2a) $AlCl_3 + BMImCl_4 \rightleftharpoons BMImAl_2Cl_7$	−32.1	−26.5	−32.8	−23.9

[1]Single point calculation, geometry optimized at the CAMB3LYP/6-31G(d) level of theory.
[2]Single point calculation, geometry optimized at the PBE0/6-31G(d) level of theory.
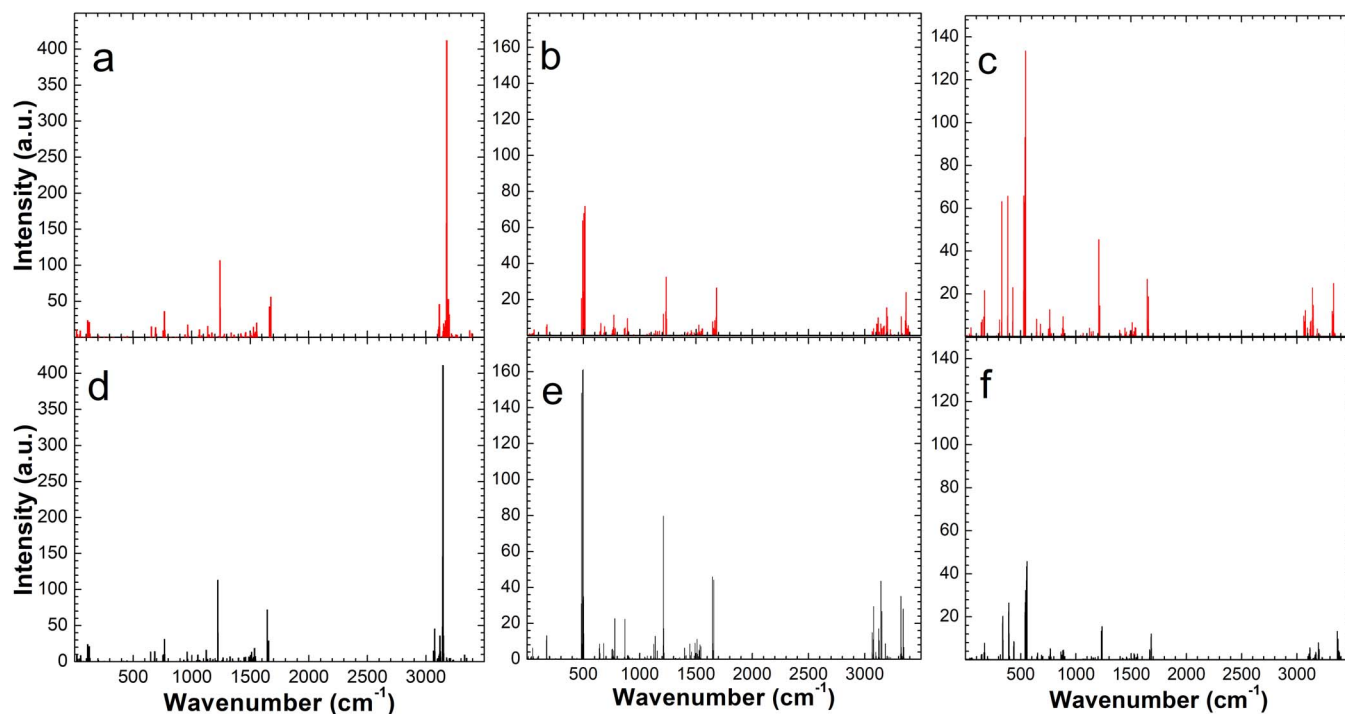
Figure 9. Weighted vibrational spectra of *BMImCl* (a,d), *BMImAlCl$_4$* (b,e) and *BMImAl$_2$Cl$_7$* (c,f) as calculated with the CAM-B3LYP (a,b,c) and PBE0 (d,e,f) functionals.

1a, we note that the presence of a cation *BMIm$^+$* enhances destabilization of the *AlCl$_4^-$* species into bulk solution. This result is observed for both the functionals and is confirmed by the MP2 calculations. In spite of such destabilization, according to the reaction free energy of the Reaction 1a, the equilibrium appears to be completely shifted toward the formation of the *AlCl$_4^-$* species. As a matter of fact, this would be dramatic in principle, because the electrochemically active species to the cathode is *Al$_2$Cl$_7^-$* rather than *AlCl$_4^-$*. However, the very low (negative) reaction free energy of the competing Reactions 2 and 2a both point to an almost complete formation of the dimeric species, at the expense of *AlCl$_4^-$*. This is confirmed by calculations to all levels of theory employed in the present work. It is worth noting that the *BMIm$^+$* cation does not affect significantly the equilibrium 2, as the differences in the reaction free energies computed with and without the *BMIm$^+$* cation (Reactions 2 and 2a in Table II) are of the order or below 1 kcal/mol. This is indeed a very important result, because it outlines the strong stability of the dimeric species with respect to the monomeric forms of aluminum present in the *BMImCl/AlCl$_3$* solutions.

Weighted IR spectrum.—Figure 9 reports calculated vibrational spectra, bar graphs, of the species *BMIm$^+$Cl$^-$* Figures 9a, 9d, *BMIm$^+$AlCl$_4^-$* Figures 9b, 9e and *BMIm$^+$Al$_2$Cl$_7^-$* Figures 9c, 9f. For each species *i*, vibrational spectra have been calculated as an equilibrium average, weighting the spectrum of the optimized configuration *j* according to its equilibrium normalized probability, proportional to $e^{-\beta G_{ij}^0}$. Data relative to CAM-B3LYP and PBE0 functionals are reported respectively in top (a,b,c panels) and bottom (d,e,f panels) Figure 9. From a qualitative point of view, for all species, a substantial overlap and mutual consistency is observed between the spectra obtained by the two different functionals. Indeed, the main difference is the absolute value of the intensity of the IR peaks obtained by means of the two functionals. These yield the same intensity for *BMImCl* (Figures 9a, 9d). On the contrary, for *BMImAlCl$_4$* the CAM-B3LYP yield lower peak intensity than PBE0, while for *BMImAl$_2$Cl$_7$* the latter yields a higher intensity.[25,26]

Conclusions

The role played by 1-Butyl-3-methylimidazolium (BMIm) chloride ionic liquid in the electrodeposition of aluminum has been studied computationally assuming a mechanism based on four elementary reaction steps. Our free energy calculations predict a strong stability of *AlCl$_4^-$* with respect to the neutral species *AlCl$_3$* into bulk solution. This would point to a low efficiency of the reduction process to the cathode, as *AlCl$_3$* would be subtracted to the equilibrium leading to the formation of the electrochemically active species *Al$_2$Cl$_7^-$*. The effect of the *BMIm$^+$* cation is to reduce significantly the stability of *AlCl$_4^-$*, even if the reaction *BMImCl + AlCl$_3$ ⇌ BMImAlCl$_4$* is always completely shifted toward the formation of the *AlCl$_4^-$* species. The scenario is inverted when focusing on the equilibrium *AlCl$_4^- + AlCl$_3$ ⇌ Al$_2$Cl$_7^-$*. In fact, in this case, the reaction free energy lies around −30 kJ/mol and hence it results much more favorable to the formation of the dimeric species. Such an outcome is confirmed by all the levels of theory adopted in this study. Moreover, it is worthwhile to note that the *BMIm$^+$* cation leaves almost unchanged the above equilibrium. This result is fully consistent with former observations, as it gives due reason for the direct formation of the aluminum metal deposit upon electroreduction.[27–29] Remarkably, as noted above, this picture is obtained both by using DFT based calculations at the levels CAMB3LYP/6-31G(d) and PBE0/6-31G(d), with full optimization and Hessian calculation of various structures corresponding to local minimum of the potential energy surface. The reaction free energies have also been calculated at the MP2/6-31G(d) level of the theory. The agreement obtained with the DFT-based calculations provides a reasonable solid ground cross-check of our modelistic approach.

ORCID

Massimo Innocenti https://orcid.org/0000-0003-1044-5583
Claudio Fontanesi https://orcid.org/0000-0002-1183-2406

References

1. Kai Grjotheim and Halvor Kvande, *Introduction to aluminum electrolysis: understanding the Hall-Heroult process*, p. 260, Aluminium-Verlag, Dusseldorf (1993).
2. S. Takahashi, N. Koura, S. Kohara, M.-L. Saboungi, and L. a. Curtiss, *Plasmas & Ions*, **2**, 91 (1999).
3. A. P. Abbott, R. C. Harris, Y.-T. Hsieh, K. S. Ryder, and I.-W. Sun, *Physical Chemistry Chemical Physics: PCCP*, **16**, 14675 (2014).
4. Y. Fang et al., *Electrochimica Acta*, **160**, 82 (2015).
5. G. Pulletikurthi, B. Bödecker, A. Borodin, B. Weidenfeller, and F. Endres, *Progress in Natural Science: Materials International*, **25**, 603 (2015).
6. C. J. Su, Y. T. Hsieh, C. C. Chen, and I. W. Sun, *Electrochemistry Communications*, **34**, 170 (2013).
7. A. Endo, M. Miyake, and T. Hirato, *Electrochimica Acta*, **137**, 470 (2014).
8. Q. Wang, B. Chen, Q. Zhang, X. Lu, and S. Zhang, *ChemElectroChem*, **2**, 1794 (2015).
9. Q. Wang, Q. Zhang, B. Chen, X. Lu, and S. Zhang, *Journal of the Electrochemical Society*, **162**, D320 (2015).
10. M. S. Al Farisi, S. Hertel, M. Wiemer, and T. Otto, *Micromachines*, **9**, 589 (2018).
11. B. Wu, R. G. Reddy, and R. D. Rogers, in *Essential Readings in Light Metals: Volume 2 Aluminum Reduction Technology*, G. Bearne, M. Dupuis, and G. Tarcy, Editors, p. 1100, Springer International Publishing, *Cham* (2016).
12. E. Guinea et al., *ChemistryOpen*, **8**, 1094 (2019).
13. J.-K. Chang, S.-Y. Chen, W.-T. Tsai, M.-J. Deng, and I.-W. Sun, *Electrochemistry Communications*, **9**, 1602 (2007).
14. U. Bardi et al., *Surface and Coatings Technology*, **203**, 1373 (2009).
15. G. Yue et al., *AIChE Journal*, **55**, 783 (2009).
16. E. Berretti et al., *Materials*, **9** (2016).
17. A. Giaccherini et al., in *ECS Transactions*, **64** (2015).
18. A. Giaccherini et al., in *Proceedings of the 2015 COMSOL Conference in Grenoble* (2015).
19. J. A. Pople, *Gaussian suite of programs*, Wallingford, Connecticut (2017).
20. T. Yanai, D. P. Tew, and N. C. Handy, *Chemical Physics Letters*, **393**, 51 (2004).
21. J. P. Perdew, M. Ernzerhof, and K. Burke, *J. Chem. Phys.*, **105**, 9982 (1996).
22. D. Chandler, *Introduction to Modern Statistical Mechanics*, p. 256, Oxford University Press, Oxford, New York (1987).
23. F. Parenti et al., *European Journal of Organic Chemistry*, **2011**, 5659 (2011).
24. D. Vanossi, L. Cigarini, A. Giaccherini, E. da Como, and C. Fontanesi, *Molecules*, **21**, 110 (2016).
25. C. Fontanesi et al., *Langmuir*, **31**, 3546 (2015).
26. P. Morvillo et al., *Polym. Chem.* (2013).
27. F. Loglio et al., *Journal of Electroanalytical Chemistry*, **575**, 161 (2005).
28. M. Innocenti et al., *Electrochimica Acta*, **50**, 1497 (2005).
29. L. Wang et al., *ChemCatChem*, **7**, 2214 (2015).